# Collaborative Caching and Reconfigurable Intelligent Surface for the Sub-THz Mobile System

Hadeel Obaid *Student Member, IEEE*, Yongxu Zhu *Senior Member, IEEE*, Bo Tan *Member, IEEE*

***Abstract*—Enabling high-speed data services with minimal latency over high spectrums represents the evolution direction of the 6G system. This letter introduces a framework for enhancing wireless communication networks and addressing the limitation of the dynamic information accessing and blockage effect through the synergy of caching strategies and reconfigurable intelligent surfaces (RIS) on the sub-Terahertz (sub-THz) frequency band. We derive the achievable rate of the proposed system and show that caching the most popular content is the optimal strategy to maximize the system rate. We introduce a closed-form solution to determine the optimal user distance using a specialized form of the Lambert W function known as the r-Lambert W function.**

***Index Terms*—Tera-hertz (THz), Reconfigurable Intelligent Surface (RIS), Caching Placement, r-Lambert W Function.**

## I. Introduction

To support immersive and interactive experiences in the envisioned 6G use cases, the mobile network is expected to provide very high-speed and low-latency data services. Therefore, the sub-Terahertz (sub-THz) bands (90∼300 GHz) are under the radar of operators and researchers due to the extremely large exploitable bandwidth. Although the sub-THz signal provides adequate bandwidth, the short transmission distance is the main hindrance to the deployment of the sub-THz communication system. The shorter link distances associated with sub-THz communications can present challenges in terms of coverage and signal attenuation over longer distances. This limitation may necessitate the deployment of dense networks or relay nodes to ensure adequate coverage. The propagation capability of the sub-THz signal is impeded by three unfavorable conditions: substantial free-space attenuation, molecular absorption, and low transmitting power. Compared to the sub-6GHz signal, the sub-THz signal experiences an additional 20 to 30 dB of attenuation on average when the distance increases from 1 to 10 meters [1]. The emitting power of a 300 GHz semiconductor-based transmitter is only around 10 mW [2], while sub-6GHz transmitters usually output more than 100 W. As a result, the sub-THz link only reaches a limited distance, for example, tens of meters [3]. To effectively utilize bandwidth resources in the sub-THz range, two strategies can be employed: firstly, bringing content closer to the user within the reachable range of the sub-THz link through caching; secondly, manipulating the signal's propagation to extend this range using beamforming and Reconfigurable Intelligent Surfaces (RIS).

Caching refers to one type of information-centric networking (ICN) mechanism in wireless communication systems. To meet high-speed and low-latency requirements, caching a portion of popular content at the network edge could obviously pare down the requirement on the costly backhaul link or reduce the fronthaul distance. In general, there are two concepts within the field of caching strategies. The coded caching aims at reducing peak traffic loads by encoding the content and the pre-caching (storing in advance) of coded content at the users' end, making data retrieval more bandwidth-efficient [4]. Another named as probabilistic caching focuses on optimizing cache utilization by prioritizing the storage of items that are most likely to be accessed frequently, thereby reducing cache misses and improving system performance. It's often used in scenarios where cache space is limited, and there is a need to dynamically adjust to changing access patterns without specific rules for item retention. An example of optimization in the transmission of popular content is the use of caching. However, even with caching, it is sometimes necessary to access the full content stored on a distant network node, such as a macro base station (MBS). This is particularly true in scenarios where the user's demand frequently changes. Ideally, this kind of data transmission over long distances would also occur over the wideband sub-terahertz (sub-THz) region. To this end, jointly improving the signal focusing level at the information source (e.g. beamforming) and optimizing the propagation (e.g. deploying of RIS) will potentially help mitigate strong atmospheric attenuation on the sub-THz band and deliver the information from the far-end information MBS to the user. In this letter, we exploit the cooperation of caching fronthaul and RIS-aided direct information accessing on the sub-THz to address the dynamics of user request and attenuation.

Recent works on RIS-aided caching systems such as [5] present an edge caching system assisted by RIS, where RIS mitigates the impact of deep fade on the offload link. In [6], RIS is adopted to improve data caching by providing additional power through wireless energy harvesting. RIS was used in [7] to improve the spectral and energy efficiency of a caching in a mobile edge computing system. However, the aforementioned works on caching and RIS cooperation are discussed in the conventional sub-6GHz frequency bands, where only limited bandwidth may lead to unsatisfied data rate and service quality. Caching and RIS on sub-THz have been studied intensively,

Manuscript received 12 January 2024; revised 5 March, 2024 and 01 June, 2024; accepted 19 July 2024. This work was supported by the Finnish Cultural Foundation/ Pirkanmaa Regional Fund. This work was also partially supported by the Information Technology Research Foundation (Tietotekniikan Tutkimussäätiö), and partially supported by the DIOR project that has received funding from the European Union's MSCA RISE programme under grant agreement No. 10100828. The associate editor coordinating the review of this article and approving it for publication was Francesco Guidi. (Corresponding author: *Yongxu Zhu*.)

H. Obaid, B. Tan are with the Unit of Electrical Engineering, Faculty of Information Technology and Communication Sciences, Tampere University, Finland (Email: {hadeel.obaid, bo.tan}@tuni.fi).

Y. Zhu is with the National Communications Research Laboratory, Southeast University, Nanjing, China (Email: yongxu.zhu@seu.edu.cn).

however, separately. While the techniques have been used previously, the cooperation of RIS and caching in the sub-THz band has not been studied fully the in literature.

In this letter, we devise an efficient information distribution scheme incorporating sub-THz underpinned caching fronthaul and RIS-aided direct information access, where integration of two supporting components: a RIS and a cache-enabled SBS, which address the dynamics of user's request and mitigate the impact of attenuation and obstacles in the propagation of the sub-THz signal, respectively. The major contribution of this work is optimizing the utilization of the cache-assisted SBS and the RIS-aided MBS links, measured by the achievable sum rate. We analyze the user location to ascertain whether the cache-assisted SBS link or RIS-aided MBS link has a more significant effect on the system performance. This is the first attempt to derive a closed-form expression for the user boundary location between RIS and SBS, using the *r-Lambert W function*. The *r-Lambert W function* is a useful tool to obtain closed-form expressions for transcendental equations that contain logarithmic and exponential functions in mathematical expression of the sub-THz propagation model. In addition, we optimize the caching placement and demonstrate that caching the most popular content (MPC) represents the optimal strategy for maximizing the system rate.

## II. System Model

We consider a THz wireless caching system assisted by a RIS, as depicted in Fig. 1. The MBS is equipped with a Uniform Linear Array (ULA) consisting of $N_{\mathrm{M}}$ elements, while the user has a single antenna. We assume the link between the user and the MBS is unavailable due to high path and penetration loss [8] caused by the long distance. To facilitate a viable MBS to user link, we incorporate two line-of-sight (LoS) components around the user: a cache-assisted SBS with a single antenna, and an RIS managed by a controller via fibers. For the SBS-to-User link, the cache-assisted SBS is equipped with a single directional antenna. It provides content stored locally, deliberately bypassing the backhaul link between the SBS and the MBS to mitigate dependence on backhaul connections, which are costly to maintain and introduce additional latency [9]. Another significant consideration of the backhaul link is the availability. Specifically, for fiber systems, should there be any interruption in the current path, the systems are designed to automatically transition to a protection path in less than 50 milliseconds [9]. Incorporating a protection path alongside the main path will result in additional costs for the backhaul deployment. For the RIS-to-User link, the RIS is configured with $N_{\mathrm{R}}$ linearly-located reflective elements are able to shift the phase of the incident signal during reflecting. It is important to note that we assume that the perfect channel state information (CSI) is available in the system.

*1) Antenna Modeling:* The response vectors of the array on the MBS and the RIS are given by

$$\mathbf{a}_{N_{\mathrm{M}}}(\vartheta_{\mathrm{D}}) = \left[1, e^{j\nu \sin\vartheta_{\mathrm{D}}}, \ldots, e^{j\nu(N_{\mathrm{M}}-1)\sin\vartheta_{\mathrm{D}}}\right], \quad (1)$$

$$\mathbf{a}_{N_{\mathrm{R}}}(\theta_{\mathrm{A/D}}) = \left[1, e^{j\nu \sin\theta_{\mathrm{A/D}}}, \ldots, e^{j\nu(N_{\mathrm{R}}-1)\sin\theta_{\mathrm{A/D}}}\right], \quad (2)$$

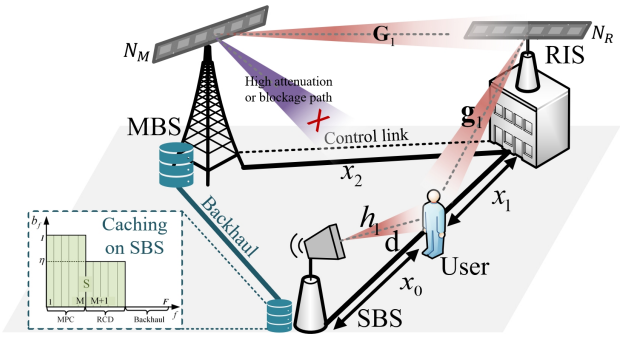


Fig. 1: System and caching model.

where $\nu = 2\pi\frac{\mathcal{D}}{\lambda}$, $\lambda$ is the wavelength, and $\mathcal{D}$ is the distance between the elements of the ULA of the MBS or the RIS, $\vartheta_{\mathrm{D}}$ indicates the angle of departure (AoD) at the MBS, $\theta_{\mathrm{A}}$ and $\theta_{\mathrm{D}}$ indicate the angle of arrival (AoA) and the AoD of the signal at the RIS. Let $\mathbf{G}_1 \in \mathbb{C}^{N_{\mathrm{R}}\times N_{\mathrm{M}}}$ be the channel matrix between MBS and RIS and can be written as

$$\mathbf{G}_1 = \mathbf{a}^H_{N_{\mathrm{R}}}(\theta_{\mathrm{A}})\mathbf{a}_{N_{\mathrm{M}}}(\vartheta_{\mathrm{D}}), \quad (3)$$

where $(.^H)$ denotes the Hermitian or the transpose conjugate. The channel vector between the RIS and the user is $\mathbf{g}_1 \in \mathbb{C}^{1\times N_{\mathrm{R}}}$ is given by

$$\mathbf{g}_1 = \mathbf{a}_{N_{\mathrm{R}}}(\theta_{\mathrm{D}}), \quad (4)$$

the channel between the user and the SBS is denoted as $\mathrm{h}_1 \in \mathbb{C}^{1\times 1}$.

*2) Sub-THz Propagation Model:* Sub-THz communication is significantly impacted by the molecular absorption loss induced by water molecules in the atmosphere, Thus, large-scale fading is characterized using a deterministic exponential power loss propagation model [10]. The notable power gap between Line of sight (LoS) and non line of sight (NLoS) paths make sub-THz channels predominantly LoS-dominant, thus rendering small-scale fading negligible [11]. Thus, THz propagation model can be written as

$$\mathcal{L}_k = \beta {x_k}^{-\alpha_{\mathrm{L}}} e^{-K(f_r)x_k}, \quad (5)$$

where $k \in (0, 1, 2)$ denote the links of SBS-to-user, RIS-to-user, and MBS-to-RIS, $\beta = (\frac{c}{4\pi f_r})^2$ is the frequency dependent coefficient, $f_r$ is the operating frequency; $c$ is the speed of light; $x_k$ is the transmission distances; $\alpha_{\mathrm{L}}$ is the path loss exponent in LoS; $K(f_r)$ represents the total molecular absorption coefficient $[m^{-1}]$ of the transmission medium, which can be calculated by the high resolution transmission molecular database.

*3) Caching Model:* we assume that $\mathcal{F} = \{1, ...f, ..., F\}$ denotes the set of $F$ files in the content database, where each file is assumed to have a normalized size of 1. We also assume that all files are sequenced according to their popularities with the *Zipf* distribution $a_f = \frac{f^{-\varepsilon}}{\sum_{f=1}^{F} f^{-\varepsilon}}$, with the most popular as the 1-th file and the least popular as the $F$-th file, where $\varepsilon$ is the *Zipf* exponent of the popularity content. The local storage size of the SBS is indicated as $S$. The content placement

probabilities $b_f$ in Fig. 1 represent the probability of the $f$-th content file being cached in the SBS:

$$b_f = \begin{cases} 1, f \in [1, M] \\ \eta, f \in [M+1, \lceil M + \frac{S-M}{\eta} \rceil] \\ 0, f \in [\lceil M + \frac{S-M}{\eta} \rceil + 1, F] \end{cases}, \quad (6)$$

where $\lceil . \rceil$ denotes the ceiling function, and $M \in (0, S]$ is allocated to store the current affairs information with certain probabilities 1, which is called the most popular contents MPC region. The remaining cache space $S - M$ allocated to randomly store contents with uniform probabilities $\eta \in (0, 1]$ is termed as Random Caching Diversity (RCD). The total caching probability can be derived as follows

$$\mathtt{P}_c = \sum\nolimits_{f=1}^{M} a_f + \sum\nolimits_{f=M+1}^{\lceil M + \frac{S-M}{\eta} \rceil} \eta \, a_f. \quad (7)$$

*4) Performance Metrics:* The received signal-to-noise ratio (SNR) of the user when sending a request for content from the SBS can be expressed as

$$\gamma_{\mathrm{S}} = \frac{P_{\mathrm{S}} \|\mathrm{h}_1\|^2 \mathcal{L}_0}{\sigma_w^2}, \quad (8)$$

where $P_{\mathrm{S}}$ is the transmit power by SBS, note that the antenna gain is factored into the transmitted power of the SBS, $\sigma_w^2$ is the noise variance at the user side, and $\|\mathrm{h}_1\|^2$ is equal to 1. The received SNR of the user when sending a request for content from the MBS can be expressed as

$$\gamma_{\mathrm{R}} = \frac{P_{\mathrm{M}} \|\mathbf{g}_1 \mathbf{\Phi} \mathbf{G}_1\|^2 \mathcal{L}_2 \mathcal{L}_1}{\sigma_w^2}, \quad (9)$$

where $P_{\mathrm{M}}$ is the MBS transmit power, $\mathbf{\Phi}$ is the phase shift introduced by the reflection of the RIS $\mathbf{\Phi} = \mathrm{diag}\{\mathbf{e}^{\mathbf{j}\phi_1}, \ldots, \mathbf{e}^{\mathbf{j}\phi_{\mathbf{N_R}}}\}$, $\phi_n \in [0, 2\pi)$. Since the antenna gain in the MBS-RIS-user link is $\mathbf{\Theta} = \|\mathbf{g_1 \Phi G_1}\|^{\mathbf{2}}$ [12, IV-A], we can expand $\mathbf{\Theta}$ to obtain the following

$$\mathbf{\Theta} = | \underbrace{\mathbf{a}_{N_{\mathrm{R}}}(\theta_{\mathrm{D}}) \, \mathbf{\Phi} \, \mathbf{a}_{N_{\mathrm{R}}}^H(\theta_{\mathrm{A}})}_{\mathbf{\Lambda_1}} |^{\mathbf{2}} \underbrace{\|\mathbf{a}_{N_{\mathrm{M}}}(\vartheta_{\mathrm{D}})\|^2}_{\mathbf{\Lambda_2}}, \quad (10)$$

where $\Lambda_2 = N_{\mathrm{M}}$ is a constant, $\Lambda_1$ can be rewrite as

$$\Lambda_1(\phi_n) = \sum\nolimits_{n=1}^{N_R} e^{j\nu(n-1)(\sin\vartheta_{\mathrm{D}} - \sin\theta_{\mathrm{A}}) + j\phi_n}. \quad (11)$$

To maximize $|\Lambda_1(\phi_n)|^2$, the optimal phase shift $\phi_n^*$ for each reflector element of the RIS [12] satisfies

$$\phi_n^* = \nu(n-1)(\sin\theta_{\mathrm{A}} - \sin\vartheta_{\mathrm{D}}), \quad (12)$$

then we have $\Lambda_1(\phi_n^*) = N_{\mathrm{R}}$ with (12), and $\mathbf{\Theta}^* = N_{\mathrm{M}} N_{\mathrm{R}}^2$. The (9) can be rewritten as

$$\gamma_{\mathrm{R}} = \frac{P_{\mathrm{M}} N_{\mathrm{M}} {N_{\mathrm{R}}}^2 \mathcal{L}_2 \mathcal{L}_1}{\sigma_w^2}. \quad (13)$$

We assume that $B$ is the system bandwidth, the overall achievable rate $\mathcal{R}_{\mathrm{C}}$ merged by $\mathcal{R}_{\mathrm{S}}$ in cache-assisted SBS link and rate $\mathcal{R}_{\mathrm{R}}$ in RIS-aided MBS link, can be obtained as

$$\mathcal{R}_{\mathrm{C}} = \underbrace{B \, \log_2(1 + \gamma_{\mathrm{S}})}_{\mathcal{R}_{\mathrm{S}}} \mathtt{P}_c + \underbrace{B \, \log_2(1 + \gamma_{\mathrm{R}})}_{\mathcal{R}_{\mathrm{R}}} (1 - \mathtt{P}_c). \quad (14)$$

## III. Problem Formulation and Optimization Development

In this section, we analyze the impact of the user's location on the utilization of cache-assisted SBS and RIS-aided MBS links of the proposed system. Then, we optimize the content placement to maximize the achievable rate.

### A. Caching decision mechanism

Here we analyze the impact of the user's location on the cache-assisted SBS and RIS-aided MBS links to the overall system performance in terms of the sum achievable data rate. First, we assume a fixed distance $d = x_0 + x_1$ between the SBS and the RIS, and the user moves along this line.

***Lemma 1:*** Initiating a connection with the cache-assisted SBS relies on the distance between the user and the SBS, specifically if the distance is within the interval $x_0 \in (0, x_0^\star]$. Should the distance extend beyond this range, $x_0 \in (x_0^\star, d]$, the user is compelled to retrieve content from the MBS via the RIS links. The boundary distance $x_0^\star$ is determined as follows

$$x_0^\star = \frac{\alpha_{\mathrm{L}} \times W_{\left(\frac{e^{dK(f_r)}}{\Lambda}\right)^{\frac{1}{\alpha_{\mathrm{L}}}}} \left( \frac{2dK(f_r)}{\alpha_{\mathrm{L}}} \left( \frac{e^{dK(f_r)}}{\Lambda} \right)^{\frac{1}{\alpha_{\mathrm{L}}}} \right)}{2K(f_r)}, \quad (15)$$

where $W_r(.)$ indicates the *Generalized $r$-Lambert W function* (GLW) [1] [13, Therom 3].

***Proof 1:*** We evaluate the robust link based on the location of the user using the equation $\Delta\mathcal{R} = \mathcal{R}_{\mathrm{S}} - \mathcal{R}_{\mathrm{R}}$, where $\mathcal{R}_{\mathrm{S}}(x_0)$ and $\mathcal{R}_{\mathrm{R}}(d - x_0)$ are present in (14). Then to find $x_0$, we set $\Delta\mathcal{R}(x_0) = 0$

$$\left( \frac{x_0}{d - x_0} \right)^{-\alpha_{\mathrm{L}}} e^{-2K(f_r)x_0} = \underbrace{\frac{P_{\mathrm{M}} \mathcal{L}_2 {N_{\mathrm{R}}}^2 N_{\mathrm{M}}}{P_{\mathrm{S}}}}_{\Lambda} e^{-dK(f_r)}, \quad (16)$$

after exponent both side to the power $-1/\alpha_{\mathrm{L}}$, we obtain:

$$\frac{x_0}{x_0 - d} \, e^{\frac{2K(f_r)x_0}{\alpha_{\mathrm{L}}}} = -\left( \frac{e^{dK(f_r)}}{\Lambda} \right)^{1/\alpha_L}, \quad (17)$$

by assuming $\mu = \frac{2K(f_r)x_0}{\alpha_{\mathrm{L}}}$ and after some algebraic manipulations, we obtain

$$\frac{\mu - 0}{\mu - \frac{2dK(f_r)}{\alpha_{\mathrm{L}}}} \, e^{\mu} = -\left( \frac{e^{dK(f_r)}}{\Lambda} \right)^{1/\alpha_{\mathrm{L}}}, \quad (18)$$

since the format in (18) accord with standard GLW function $W\left( \frac{(x-t)\ldots(x-t_n)}{(x-s)\ldots(x-s_n)} e^x = a \right)$ which has the solution $W\left( \begin{matrix} t..t_n \\ s..s_n \end{matrix} ; a \right)$ [13], we can find the exact solution of $x_o^\star$ in the transcendental equation (18) as

$$x_o^\star = \frac{\alpha_{\mathrm{L}}}{2K(f_r)} W\left( \begin{matrix} 0 \\ \frac{2dK(f_r)}{\alpha_{\mathrm{L}}} \end{matrix} ; -\left( \frac{e^{dK(f_r)}}{\Lambda} \right)^{1/\alpha_{\mathrm{L}}} \right), \quad (19)$$

on top of that, since our GLW has only one upper parameter $t$ and one lower parameter $s$, (18) can be identified as the

[1]Note that $W_r()$ is the special case of Generalized Lambert function [13], which has gained recognition as an effective solution for addressing various physical problems (such as molecular physics, water waves, and electromagnetic materials) where the classical Lambert W function is insufficient.

Generalized r-Lambert function ($W_r$) that satisfies $xe^x + rx = a$, where

$$W\left(\begin{array}{c} t \\ s \end{array}; a\right) = t + W_{-ae^{-t}}\left(ae^{-t}(t-s)\right), \tag{20}$$

herein $r = -ae^{-t}$ and $t = 0$ in our case. Thus, the exact solution of $x_0$ in (18) can be expressed as in (15), which completes the proof. □

### B. Optimal Content Placement

Considering the conditions where $x_0$ falls within the interval $(0, x_0^*]$ and $\mathcal{R}_\mathrm{S} > \mathcal{R}_\mathrm{R}$, our objective is to enhance the system's total achievable rate $\mathcal{R}_\mathrm{C}$ by optimizing the content placement $\eta$ and $M$. The problem formulation can be expressed as

$$\begin{aligned} \mathbb{P}_1 \ & \max_{M,\eta} \ \mathcal{R}_\mathrm{C} \text{ in (14)} \\ & \text{s.t.} \quad \eta \in (0,1] \ , \ M \in [0, S]. \end{aligned} \tag{21}$$

***Lemma 2:*** To maximize $\mathcal{R}_\mathrm{C}$, caching MPC is the optimal solution, i.e. $M^* = S$, and the optimal caching placement probability $\eta = 1$. Then the optimized $\mathtt{P}_\mathrm{C}$ in $\mathcal{R}_\mathrm{C}$ can be expressed as

$$\mathtt{P}_\mathcal{C}^* = \frac{S^{1-\varepsilon} - 1}{F^{1-\varepsilon} - 1}. \tag{22}$$

***Proof 2:*** First we apply the integral approximation as in [14] to derive $\mathtt{P}_c$ as

$$\mathtt{P}_c \approx \frac{(1-\eta)M^{1-\varepsilon} + \eta\left[M + \frac{S-M}{\eta}\right]^{1-\varepsilon} - 1}{F^{1-\varepsilon} - 1}. \tag{23}$$

Then we take the first-order derivative of $\mathcal{R}_\mathrm{C}$ with respect to $M$ as

$$\begin{aligned} \frac{\partial \mathcal{R}_\mathrm{C}(M)}{\partial M} &= \frac{\Delta\mathcal{R}}{F^{1-\varepsilon} - 1} \\ &\times (1-\varepsilon)(1-\eta)\left[M^{-\varepsilon} - \left(M + \frac{S-M}{\eta}\right)^{-\varepsilon}\right], \end{aligned} \tag{24}$$

also, we take the first-order derivative of $\mathcal{R}_\mathrm{C}$ with respect to $M$

$$\begin{aligned} \frac{\partial \mathcal{R}_\mathrm{C}(\eta)}{\partial \eta} = \frac{\Delta\mathcal{R}}{F^{(1-\varepsilon)} - 1}\Bigg[-M^{1-\epsilon} + \left(M + \frac{(S-M)}{\eta}\right)^{(1-\epsilon)} \\ - \frac{(S-M)(1-\epsilon)(M + \frac{(S-M)}{\eta})^{-\epsilon}}{\eta}\Bigg]. \end{aligned} \tag{25}$$

It can be observed from the analysis of (25) and (24) that both $\frac{\partial \mathcal{R}_\mathrm{C}(M)}{\partial M}$ and $\frac{\partial \mathcal{R}_\mathrm{C}(\eta)}{\partial \eta}$ yield positive values. This positivity holds whether $\varepsilon < 1$ or $\varepsilon > 1$. Knowing that $\Delta\mathcal{R} > 0$, it follows that $\frac{\partial \mathcal{R}_\mathrm{C}(M)}{\partial M} \geq 0$ and $\frac{\partial \mathcal{R}_\mathrm{C}(\eta)}{\partial \eta} \geq 0$. Under these conditions, $\mathcal{R}_\mathcal{C}$ is a monotonically increasing function of $M \in [0, S]$ and $\eta \in (0, 1]$. Therefore, the optimal values can be obtained at the boundary of these intervals, by setting $M = S$ and $\eta = 1$, the proof is complete.

□

Based on ***Lemma 1*** and ***Lemma 2***, we can rewrite the overall achievable rate in (14) as

$$\mathcal{R}_\mathrm{C} = \begin{cases} \mathcal{R}_\mathrm{S}\frac{S^{1-\varepsilon}-1}{F^{1-\varepsilon}-1} + \mathcal{R}_\mathrm{R}\frac{F^{1-\varepsilon}-S^{1-\varepsilon}}{F^{1-\varepsilon}-1}, & x_0 \leq x_0^\star \\ \mathcal{R}_\mathrm{R}, & x_0^\star \leq x_o < d \end{cases}, \tag{26}$$

when $x_0$ is in the range $(0, x_0^\star]$, both links can serve the user based on the requested content. If $x_0$ falls within $[x_0^\star, d)$, the cache-assisted SBS link offers no additional benefit.

## IV. Numerical Results and Discussion

This section evaluates the performance of the proposed caching scheme by presenting numerical results. TABLE I lists the system parameters unless otherwise specified.

TABLE I. SYSTEM PARAMETER VALUES.

| Parameters | Values |
|---|---|
| SBS caching capacity ($S$) | 100 |
| Content library size (F) | $10^4$ |
| Path loss exponent ($\alpha_\mathrm{L}$) [15] | 2 |
| Available bandwidth in THz [2] | 10 GHz |
| Molecular absorption coefficient $K(f_r)$ [2] | 0.0033 |
| Operating frequency | 0.3 THz |
| Transmit power at SBS & MBS [2] | 10 & 20 dBm |
| Number of transmitter antennas ($N_\mathrm{M}$) | 32 |
| Number of reflector elements ($N_\mathrm{R}$) | 64 |
| The noise power ($\sigma_w^2$) | -74 dBm |

In Fig. 2, the average achievable rate is obtained from (14) is explored against the content placement probability. It can be observed that the system achievable rate is a monotonically increasing function of the caching placement probability. It is important to note that the Monte Carlo simulations match perfectly with analytical results. The figure also investigates the impact of varying the parameter $\epsilon$ on the achievable rate. It is noted that the achievable rate is higher when $\epsilon$ is higher, indicating that the requested contents have a higher probability of being connected between the SBS and the user.

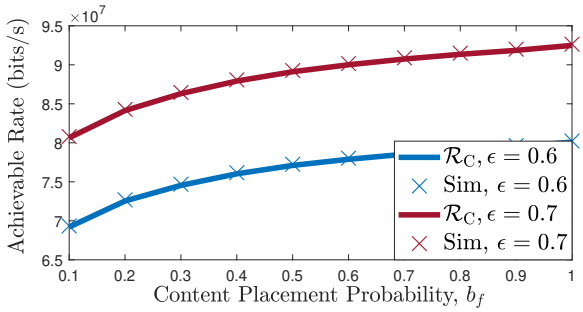


Fig. 2: The achievable rate versus $b_f$.

In Fig. 3 (a), (b), and (c), the average achievable rate is obtained from (26). In Fig. 3 (b), it is observed that as the size of the content library $F$ increases, there is a corresponding decline in the rate, showcasing the impact of a larger pool of content on the communication efficiency. This decline is evident across various values of $\varepsilon$, highlighting the importance of managing the content library size for optimizing communication performance in practical scenarios. Furthermore, Fig. 3 (c) illustrates a positive correlation between the rate and the number of reflecting elements of the RIS denoted as $N_L$. As the number of reflecting elements increases, the rate increases, emphasizing the role of RIS configuration in enhancing the communication throughput.These results show that managing the cache storages and tuning RISs configuration help to

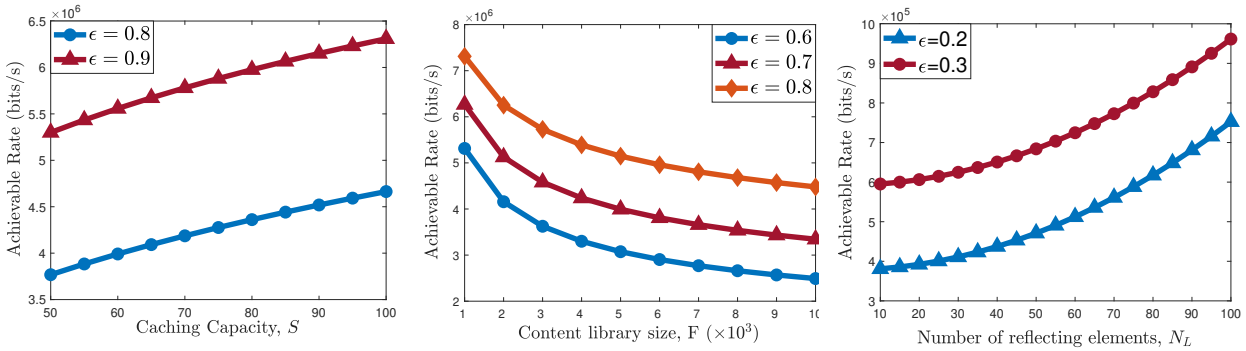


(a) (b) (c)

Fig. 3: a) The achievable rate versus $S$. b) The achievable rate versus $F$. c) The achievable rate versus $N_L$. Where $d = 40$ m, $x_2 = 10$ m, $x_o^\star = 36.6$ m.

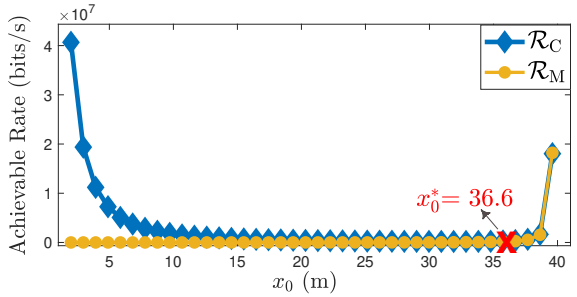


Fig. 4: The achievable rate versus $x_0$, where $\epsilon = 0.1$, $\eta = 1$, $d = 40$ m, $x_2 = 10$ m.

effectively exploit the sub-THz bandwidth resource for high-speed communications.

Fig. 4 effectively visualizes the relationship between the achievable rate and the distance $x_0$ over a fixed distance between the RIS and the SBS, as shown in (26). It is observed that the system exhibits an increased rate under two key conditions: when the user is in close proximity to the SBS or near the RIS. The optimal value of $x_0$, denoted as $x_0^\star$, is determined numerically using (15). Beyond the boundary point $x_0^\star$, the user's connection relies solely on the RIS links associated with $\mathcal{R}_\mathrm{R}$.

## V. Conclusion

In this letter, we introduced a framework to enhance wireless communication networks by incorporating caching and RIS in sub-THz transmission. The approach exploits the bandwidth resources of the sub-THz band, addresses the dynamics of user's request, and mitigates the impact of attenuation and obstacles in the propagation of the sub-THz signal. Based on the derived achievable rate of the proposed RIS-aided THz wireless caching system, we provided a closed-form solution to determine the optimal user distance by using the *r-Lambert W function*. We then use theoretical formulation and optimization to confirm that caching MPC in the SBS is the optimal content placement strategy. Through numerical results, we have investigated the impact of the system's parameters on the achievable rate. The collaboration of caching and RIS in the sub-THz transmission promises enhancements in the data rates and latency, emphasizing its potential for future advancements in 6G networks. The proposed system could be extended to support multi-user scenarios and examine the effects of user mobility on the performance of the proposed system. In addition, the potential of cooperative caching strategies among multiple SBSs could be investigated, which could lead to more efficient use of storage resources and better load balancing across the network.

## References


[1] A.-A. A. Boulogeorgos and et al., "Performance evaluation of thz wireless systems operating in 275-400 ghz band," in *87th IEEE VTC Spring*, 2018, pp. 1–5.

[2] K. Dovelos, S. D. Assimonis, H. Quoc Ngo, B. Bellalta, and M. Matthaiou, "Intelligent reflecting surfaces at terahertz bands: Channel modeling and analysis," in *IEEE International Conference on Communications Workshops (ICC Workshops)*, 2021, pp. 1–6.

[3] T. Harter and et al., "Wireless thz link with optoelectronic transmitter and receiver," *Optica*, vol. 6, no. 8, pp. 1063–1070, 2019.

[4] X. Xu and M. Tao, "Modeling, analysis, and optimization of coded caching in small-cell networks," *IEEE Transactions on Communications*, vol. 65, no. 8, pp. 3415–3428, 2017.

[5] Y. Chen, M. Wen, E. Basar, Y.-C. Wu, L. Wang, and W. Liu, "Exploiting reconfigurable intelligent surfaces in edge caching: Joint hybrid beamforming and content placement optimization," *IEEE Trans. Wireless Commun.*, vol. 20, no. 12, pp. 7799–7812, 2021.

[6] Z. Chu and et al., "Intelligent-reflecting-surface-empowered wireless-powered caching networks," *IEEE Internet Things J.*, vol. 9, no. 15, pp. 13 153–13 167, 2022.

[7] J. Zhang, R. Wang, J. Wu, and L. Ai, "Cache-aided mec with the assistance of intelligent reflecting surface," *IEEE Internet of Things Journal*, vol. 10, no. 19, pp. 16 686–16 699, 2023.

[8] H. Du, J. Zhang, K. Guan, D. Niyato, H. Jiao, Z. Wang, and T. Kürner, "Performance and optimization of reconfigurable intelligent surface aided thz communications," *IEEE Trans. Commun.*, vol. 70, no. 5, pp. 3575–3593, 2022.

[9] A. Haidine and A. Aqqal, "Broadband communications networks: Recent advances and lessons from practice," 2018.

[10] N. Kouzayha, M. A. Kishk, H. Sarieddeen, M.-S. Alouini, and T. Y. Al-Naffouri, "Coexisting terahertz and rf finite wireless networks: Coverage and rate analysis," *IEEE Trans. Wireless Commun.*, 2022.

[11] X. Wang, Z. Lin, F. Lin, and L. Hanzo, "Joint hybrid 3d beamforming relying on sensor-based training for reconfigurable intelligent surface aided terahertz-based multiuser massive mimo systems," *IEEE Sensors Journal*, vol. 22, no. 14, pp. 14 540–14 552, 2022.

[12] Y. Han, W. Tang, S. Jin, C.-K. Wen, and X. Ma, "Large intelligent surface-assisted wireless communication exploiting statistical CSI," *IEEE Trans. Veh. Technol.*, vol. 68, no. 8, pp. 8238–8242, 2019.

[13] I. Mező and Á. Baricz, "On the generalization of the lambert function," *Transactions of the American Mathematical Society*, vol. 369, no. 11, pp. 7917–7934, 2017.

[14] Y. Zhu, G. Zheng, L. Wang, K.-K. Wong, and L. Zhao, "Content placement in cache-enabled sub-6 ghz and millimeter-wave multi-antenna dense small cell networks," *IEEE Trans. Wireless Commun.*, vol. 17, no. 5, pp. 2843–2856, 2018.

[15] Z. Lin, L. Wang, B. Tan, and X. Li, "Spatial-spectral terahertz networks," *IEEE Trans. Wireless Commun.*, vol. 21, no. 6, pp. 3881–3892, 2021.